Journal of Crystal Growth 660 (2025) 128157

Contents lists available at ScienceDirect

Journal of Crystal Growth

journal homepage: www.elsevier.com/locate/jcrysgro

Effects of synthesis methods on the structural and magnetic properties of $Mg_{0.2}Ni_{0.6}Zn_{0.2}Fe_2O_4$ spinel ferrite

Sarang R. Daf [a], Dilip S. Badwaik [b,*], Shrikant M. Suryawanshi [b], Bhupendra T. Kumbhare [a], Bhaurao R. Balbudhe [c], Rupesh S. Wandhare [d]

[a] Department of Physics, Shri Shivaji Science College, Nagpur 440012, India
[b] Department of Physics, Kamla Nehru Mahavidyalaya, Nagpur 440024, India
[c] Department of Physics, Shri Dnyanesh Mahavidyalaya Nawargaon 441223, India
[d] Department of Physics, Arts, Commerce & Science College, Maregaon 445303, India

ARTICLE INFO

Keywords:
$Mg_{0.2}Ni_{0.6}Zn_{0.2}Fe_2O_4$ spinel ferrite
Sol–gel auto-combustion
Hydrothermal
Co-precipitation

ABSTRACT

Spinel ferrite nanoparticles (SFNPs), such as $Mg_{0.2}Ni_{0.6}Zn_{0.2}Fe_2O_4$, have unique properties that are influenced by their synthesis methods. Different bottom-up approaches, including sol–gel, auto-combustion, hydrothermal, and co-precipitation method were used to prepare these nanoparticles. Structural, morphological, optical and magnetic properties were analysed using techniques like X-ray diffraction (XRD), Fourier transform infrared spectroscopy (FTIR), transmission electron microscope (TEM), scanning electron microscope (SEM) and vibrating sample magnetometer (VSM). Crystallite sizes measured using Scherrer's formula were 28.9 nm, 20.2 nm, and 7.5 nm for the respective synthesis methods. FTIR spectra indicated metal–oxygen bond formation, TEM and SEM confirms cubical shaped morphology while VSM analysis revealed the pseudo-single domain nature of the synthesized SFNPs. The observed and estimated parameter strongly suggests that these materials could be used in biomedical and electronic applications.

1. Introduction

Nanotechnology has revolutionised the field of scientific research and technology due to its extraordinary and distinctive electrical, magnetic, optical, and mechanical properties. The size of nanoparticles is a crucial property that has recently caught the attention of researchers in the field of nano-scale particles. The design of nanoscale materials with precise dimensions and morphology is a prominent aspect of nanotechnology. These materials have found applications in several sectors such as optics, electronics, and biomedicine. In the realm of Nano-science and nanotechnology, there has been significant interest in nanocrystalline magnetic materials made of iron oxide due to its exceptional ability to adjust their electrical, magnetic, and optical characteristics [1–3].

Soft ferrite is considered the optimal magnetic material due to its superior characteristics in terms of fabrication ease, affordability, and stability [4]. The primary materials of importance in the field of nanotechnology are spinel ferrites, which have the general chemical formula $M^{2+}Fe_2O_4$ (M^{2+}=Cu^{2+}, Mn^{2+}, Mg^{2+}, Zn^{2+}, Ni^{2+}, Co^{2+}, etc.). This phenomenon arises as a result of their widespread utilisation in diverse domains, including but not limited to high-capacity data storage devices, transformer cores, ferrofluids, drug delivery systems in biomedical settings, catalytic reactions, energy storage, gas sensor technology, and applications in magnetic resonance imaging (MRI), among other areas [5–8].

Pamela Yajaira Reyes-Rodrígueza et al. [9] reported synthesis of Mg-Zn spinel ferrites using sol–gel method. The $Mg_{0.9}Zn_{0.1}Fe_2O_4$ and $Mg_{0.7}Zn_{0.3}Fe_2O_4$ nanoparticles showed an average particle size of 15 nm and a near-spherical morphology. The synthesized Mg-Zn spinel ferrite materials have potential use as thermoseeds in hyperthermia treatment. Tetiana Tatarchuk et al. [10] synthesized MgZn spinel nanostructure with sol–gel auto-combustion method and studied adsorption properties along with the structural and optical properties. Adsorbent property revels Mg-Zn ferrospinels can be considered as good adsorbents can be used for wastewater purification. B. Rabi et al. [11] synthesises Ni-substituted Zn spinel ferrites by co-precipitation method. they reported UV–VIS analysis with optical energy band gaps through Tauc plots, do not exceed 5 eV which confirms the semiconductor nature of

* Corresponding author.
E-mail address: badwaik_ds@rediffmail.com (D.S. Badwaik).

https://doi.org/10.1016/j.jcrysgro.2025.128157
Received 8 February 2025; Received in revised form 15 March 2025; Accepted 19 March 2025
Available online 20 March 2025

our samples. This semiconductor property is looked after for the fabrication of microelectronic devices. Rohit Jasrotia et al. [12] synthesizes NiZn nanosized spinel ferrites with a soft magnetic nature. They concluded that the synthesized NiCu could be more fascinatedly applicable for high frequency and multi-layer chip inductors (MLCIs) applications. Therefore, the complex Mg-Ni-Zn ferrites with a spinel structure may have desirable properties and utilizes, such as high-frequency and multi-layer chip inductors (MLCIs), thermoseeds in hyperthermia treatment adsorbents that can be used for wastewater purification, and the fabrication of microelectronic devices. Hence an attempt was made to synthesise Mg-Ni-Zn spinel ferrite which will shows both biomedical as well as electronics and technological applications.

It has been studied that structural, morphological, optical, magnetic and electrical features of ferrites are influenced by the nature of divalent cations in the spinel structure and their placement at tetrahedral and octahedral sites, as well as the synthesis mechanism and conditions, synthesis temperature, pH, and other variables [13]. Sol–gel auto-combustion involves the transformation of a solution (sol) into a gel phase and then into a solid phase (gelation and aging), typically through hydrolysis and condensation reactions [14]. Hydrothermal synthesis involves the hydrothermal reaction of precursor materials in an aqueous solution at elevated temperatures and pressures in Teflon-coated autoclave. The hydrothermal process allows for the controlled nucleation and growth of nanoparticles, resulting in well-defined size, shape, and crystallinity [15]. In the Coprecipitation synthesis method, aqueous solutions containing the desired metal ions are mixed under controlled conditions, leading to the precipitation of nanoparticles. The co-precipitation method offers advantages such as simplicity and scalability. The precursor solutions are mixed together under controlled conditions, such as pH, temperature, and stirring rate. Typically, a base (e.g., sodium hydroxide) is added to induce precipitation by neutralizing the metal ions in solution. The addition of the base results in the formation of metal hydroxide precipitates [16].

In the present research module, we have synthesized $Mg_{0.2}Ni_{0.6}Zn_{0.2}Fe_2O_4$ spinel ferrite nanoparticles (SFNPs) with the three different bottom-up approaches of synthesis including sol–gel auto-combustion, hydrothermal and coprecipitation method and our aim is to find most suitable synthesis method for Mg-Ni-Zn SFNPs in perspective of structural, spectroscopic and magnetic parameters for suitable applications. The various structural, spectroscopic-elastic and magnetic parameters obtained from X-ray diffraction, Fourier Transforms Infrared Analysis, Vibrating Sample Magnetometer respectively were discussed and seen to be influenced by synthesis process.

2. Experimental details

All the reagents used were AR grade obtained from LOBA, India and were used as received without further purification. Sol–gel auto-combustion, hydrothermal and coprecipitation bottom-up chemical approaches were used to synthesis $Mg_{0.2}Ni_{0.6}Zn_{0.2}Fe_2O_4$ spinel ferrite nanoparticles (SFNPs). Synthesis approaches named Sol–gel auto-combustion, hydrothermal and coprecipitation were discussed in detail below.

2.1. Sol–gel auto-combustion method

The AR grade, Magnesium (II) nitrate, Nickel (II) nitrate, Zinc (II) nitrate, Iron (III) nitrate and urea were used for preparation of $Mg_{0.2}Ni_{0.6}Zn_{0.2}Fe_2O_4$ spinel ferrite nanoparticles (SFNPs). The metal nitrate precursors of Mg, Ni, Zn and Fe were employed in stoichiometric proportion as indicated in the chemical formula $Mg_{0.2}Ni_{0.6}Zn_{0.2}Fe_2O_4$ and dissolved in 50 ml double distilled water under continuous stirring at 80 °C for 30 mins to get homogeneous solution with addition of urea as fuel. After intense stirring for 30 min, a uniform solution is produced, which is then followed by the development of the gel due to the addition of urea. After a period of time, self-sustaining combustion caused the release of dark brown smoke, and the gel ignited, producing moderate flames and transforming into a foamy dark brown powder. The materials were crushed for around 160 min using a mortar pestle. This as-synthesised fine powder undergoes calcination process for 5 hrs at 800 °C in muffle furnace. The obtained dark brown coloured ferrite powder is ready for further characterizations.

2.2. Hydrothermal method

As with the AR grade, A solution containing 0.2 M Magnesium (II) chloride, 0.2 M Nickel (II) chloride, 0.2 M Zinc (II) chloride, 0.4 M Iron (III) chloride, and 4 M sodium hydroxide was utilised to prepare $Mg_{0.2}Ni_{0.6}Zn_{0.2}Fe_2O_4$ spinel ferrite nanoparticles (SFNPs). The requisite quantities of metal chloride solutions were utilised in a stoichiometric manner to achieve the target composition of $Mg_{0.2}Ni_{0.6}Zn_{0.2}Fe_2O_4$. Precipitation of the precursors occurred as a result of neutralisation using 4 M sodium hydroxide solutions. During the precipitation, the pH was adjusted to a value of 12 in order to guarantee the completion of the precipitation process. Deionized water was added to the precipitate in order to fill the Teflon Coated Autoclave up to 70 % of its capacity. The slurry was subjected to hydrothermal treatment at a temperature of 180 °C for 5 h (453 K) in a 200 ml stainless steel autoclave. After a duration of 20 h, the slurry was cooled to room temperature naturally, filtered, and rinsed with di-ionized water until all impurities were removed. Finally, it was dried for 2 h at 80 °C. The resulting powder has a light brown hue. The ingredients were crushed for approximately 90 min using a mortar pestle.

2.3. Coprecipitation method

The AR grade, 0.2 M Magnesium (II) chloride, 0.2 M Nickel (II) chloride, 0.2 M Zinc (II) chloride, 0.4 M Iron (III) chloride and 4 M sodium hydroxide were used for preparation of $Mg_{0.2}Ni_{0.6}Zn_{0.2}Fe_2O_4$ spinel ferrite nanoparticles (SFNPs). The precise amounts of metal chloride solutions were utilized in a stoichiometric manner to achieve the intended composition of $Mg_{0.2}Ni_{0.6}Zn_{0.2}Fe_2O_4$. Precipitation of the precursors occurred as a result of neutralisation using 4 M sodium hydroxide solutions. During the precipitation, the pH was adjusted to 12 in order to guarantee the completion of the precipitation process. Once pH 12 is obtained, the slurry so obtained were further stirred and heated constant reaction temperature (80 °C) for 1 hr. The precipitate was washed with distilled water and acetone after cooling to room temperature. The filtered precipitate was subsequently dried at 100 °C for a duration of 2 h. The resultant sample was crushed for 160 min with a mortar and pestle.

The obtained brown-coloured ferrite powder undergoes calcination at 800 °C for 5 hrs in muffle furnace. Brown-coloured ferrite powder is ready for further characterizations.

2.4. Characterization techniques

The X-ray diffraction pattern of the as-synthesized SFNPs samples was recorded using a Tabletop Rigaku Mini-Flex 600 X-ray diffractometer, Rigaku Japan. The X-ray source used was Cu-89Kα with a wavelength of 1.54059 Å. The absorption scale of 0.4 K cm-1 to 4 K cm-1 was used to study the functional group and the type of bonds present. This was done using Fourier Transform Infrared Spectroscopy (FTIR) with the Bruker Alpha model. The magnetic properties of the synthesised SFNPs were examined using a Vibrating Sample Magnetometer (VSM) from the Lakeshore 7400 series.

3. Results and discussion

3.1. X-ray diffraction analysis

The X-ray diffraction pattern of as-synthesized $Mg_{0.2}Ni_{0.6}Zn_{0.2}Fe_2O_4$

spinel ferrite nanoparticles (SFNPs) by sol–gel auto-combustion, hydrothermal and coprecipitation method are shown in Fig. 1. The indexed peaks of (220), (311), (400), (333) and (440) shows the formation of single phase cubic f.c.c. structured spinel ferrite nanoparticles (SFNPs) with the space group Fd-3 m. Intensity of (311) peak is highest as compared to other peaks. Moreover the intensity of the diffraction peak of spinel ferrite at (311) plane was considered as a measure of its degree of crystallinity [17].

In the present XRD study, it has been observed that the synthesis method modifies the value of intensity, lattice dimension (a), Bragg's angle (2θ) and FWHM (β) which will affect the size of crystallite (D) and other structural parameters like strain (ε), dislocation density (δ), interplanar spacing (d) and X-ray density ($\rho_{X\text{-ray}}$) were calculated [18] as mentioned in Table 1.

The lattice dimension (a) of synthesized SFNPs is calculated using the equation below.

$$a = d_{hkl}\sqrt{h^2 + k^2 + l^2} \tag{1}$$

Lattice dimension *(a)* found to be 8.422 Å, 8.419 Å, 8.379 Å for sol–gel auto-combustion, hydrothermal and coprecipitation synthesis approach (Table 2) which is in good agreement with earlier reported literature for Mg-Ni-Zn soft ferrites [19–21].

The crystallite size calculated using X-ray peak broadening of most intense (311) peak in Eq. (2),

$$D = \frac{0.9\lambda}{\beta}\left(\frac{1}{Cos\theta}\right) \tag{2}$$

The crystallite size calculated using Scherrer formula is found to be 28.9 nm for solgel auto-combustion method, 20.2 nm for hydrothermal method while the lowest 7.5 nm were found for coprecipitation method. The results revealed that at high temperature in solgel auto-combustion method favours the growth of the crystallite size at the nucleation centers, thus conforming to the larger dimension of lattice parameters and crystallite size as compared to hydrothermal method and coprecipitation method respectively [17].

The induced microstrain for synthesized SFNPs can be calculated by given equation

$$The\ \text{microstrain}(\varepsilon) = \frac{\beta}{4\tan\theta} \tag{3}$$

The dislocation in the lattice site can be estimated by the relation.

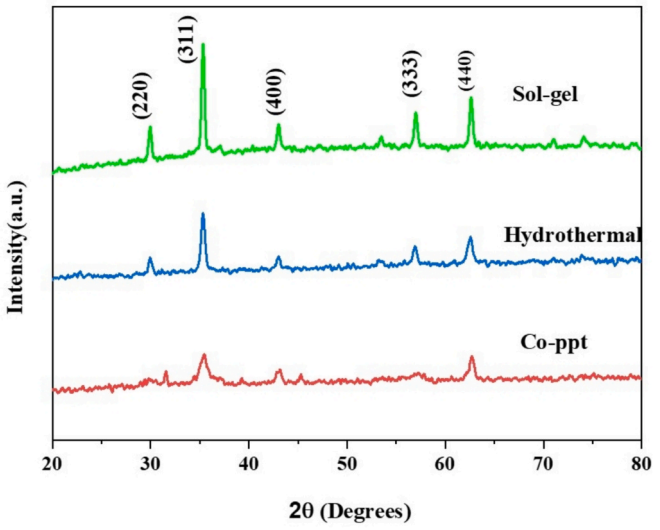

Fig. 1. XRD patterns of $Mg_{0.2}Ni_{0.6}Zn_{0.2}Fe_2O_4$ SFNPs synthesized with different synthesis approaches.

$$Dislocation density(\delta) = {}^{1}/_{D^2} \tag{4}$$

The X-ray density of synthesized NPs can be evaluated by the relation

$$\rho_{X-ray} = \frac{ZM}{N_A a^3} \tag{5}$$

where, $N_A = 6.02 \times 10^{23}$ mol/gm is Avogadro's number, M specifies the molecular weight of synthesized $Mg_{0.2}Ni_{0.6}Zn_{0.2}Fe_2O_4$ SFNPs and Z (For spinel ferrite Z = 8) is the number of molecules per unit cell.

It is evident from Table 1 to that all the structural parameters reported for synthesized SFNPs show variation in their values which is attributed to different approaches utilised for synthesis of SFNPs.

3.2. Vibrational Spectroscopy

Fourier-transform infrared (FTIR) spectrum was obtained to determine the metal–oxygen functional groups existing in the $Mg_{0.2}Ni_{0.6}Zn_{0.2}Fe_2O_4$ SFNPs synthesized with different synthesis approaches. The FTIR spectra of synthesized SFNP are illustrated in Fig. 2. The occurrence of two distinct highs, ν_1 and ν_2, in all the samples can be attributed to the stretching and bending vibrations of the metal–oxygen bonds. This confirms the production of spinel ferrite [22,23]. There was a clear peak at 457–468 cm^{-1} for synthesized $Mg_{0.2}Ni_{0.6}Zn_{0.2}Fe_2O_4$ SFNPs, which corresponds to the Fe-O stretching movement mode of the tetrahedral sub-lattice caused by the distribution of Fe^{3+} ions at tetrahedral sites. On the other hand, the peak at 486–493 cm^{-1} was caused by the seismic mode of the octahedral sub-lattice in the spinel structure. An extending vibration's absorption region in an infrared spectrum is predicted by Hooke's law to relies on the bond energy and the masses of the ions interconnected by the connection [24].

The binding strength known as the force constant is given by Eq. (6) below

$$K = 4\pi^2 \nu^2 C^2 \mu \tag{6}$$

In this case, K stands for the force constant. The speed of light is signified by C, and ν is wave number of particular vibration band. μ represents the reduced mass of the Fe-O bond. For the sol–gel method sample, the tetrahedral (A-O) and octahedral (B-O) force constants are 1.735 × 10^2N/m and 1.535 × 10^2N/m, respectively. For the hydrothermally synthesized sample, they are 1.794 × 10^2N/m and 1.549 × 10^2N/m, For the co-precipitation technique the values are 1.779 × 10^2N/m and 1.605 × 10^2N/m, respectively. The change in positional band in samples is responsible for the difference in the value of the force constant [25].

Debye temperature (θ_D) given by Eq. (7) impacts thermodynamic properties like mean square atomic displacement, specific heat, melting temperature, vibrational energy, and elastic constant [26].

$$\theta_D = \frac{(hC\nu_{av})}{2\pi K} \tag{7}$$

From Table 3 There is slight increase in θ_D, with different synthesis approaches, which suggests enhancement of the lattice vibrations and the obtained values of are consistent with previously published results [27–29].

3.3. Magnetic properties

The magnetic properties of $Mg_{0.2}Ni_{0.6}Zn_{0.2}Fe_2O_4$ spinel ferrite nanoparticles (SFNPs) synthesised using sol–gel auto-combustion, hydrothermal, and coprecipitation methods were investigated utilising M−H responses at room temperature, as depicted in Fig. 5. Table 3 displays the measured values of several magnetic properties obtained from hysteresis loops, such as coercivity (*Hc*), retentivity (*Mr*) saturation magnetization (*Ms*), squareness ratio, and magnetic moment. Table 3 illustrates the impact of synthesis methods on various magnetic

Table 1
Peak Position (2θ), lattice dimension (a), crystallite size (D), strain (ε), dislocation density (δ), Interplaner spacing (d) and X-ray density ($\rho_{x\text{-}ray}$) of $Mg_{0.2}Ni_{0.6}Zn_{0.2}Fe_2O_4$ SFNPs synthesized with different synthesis approaches.

Sr.No	Synthesis approach	2θ(deg.)	a (Å)	$D \times 10^{-9}$ (m)	$\varepsilon \times 10^{-3}$	$\delta^{2}_{lines/m} \times 10^{15}$	β(deg)	d-spacing (Å)	ρ_{X-ray}(g/cm^3)
1	Sol–gel	35.32	8.422	28.9	4.139	1.312	0.302	2.539	5.042
2	Hydrothermal	35.30	8.419	20.2	5.897	2.661	0.43	2.539	5.047
3	Coprecipitation	35.48	8.379	7.5	15.001	1.738	1.10	2.527	5.118

Table 2
Tetrahedral vibration (ν_1), Octahedral vibration (ν_2), Force constant at tetrahedral and octahedral positions (K_t and K_o), and Debye Temperature (θ_D) of $Mg_{0.2}Ni_{0.6}Zn_{0.2}Fe_2O_4$ SFNPs synthesized with different synthesis approaches.

Sr.No.	Synthesis approach	ν_1 (A-Site)	ν_2 (B-Site)	$K_t \times 10^2$ (A-site)	$K_o \times 10^2$ (B-site)	Average Force Constant $K_{av}=(K_t + K_o)/2 \times 10^2$	Debye Temperature (θ_D)
1	Sol–gel	486.56	457.70	1.735	1.535	1.635	108.28
2	Hydrothermal	494.81	459.76	1.794	1.549	1.671	109.46
3	Coprecipitation	492.75	468.01	1.779	1.605	1.692	110.18

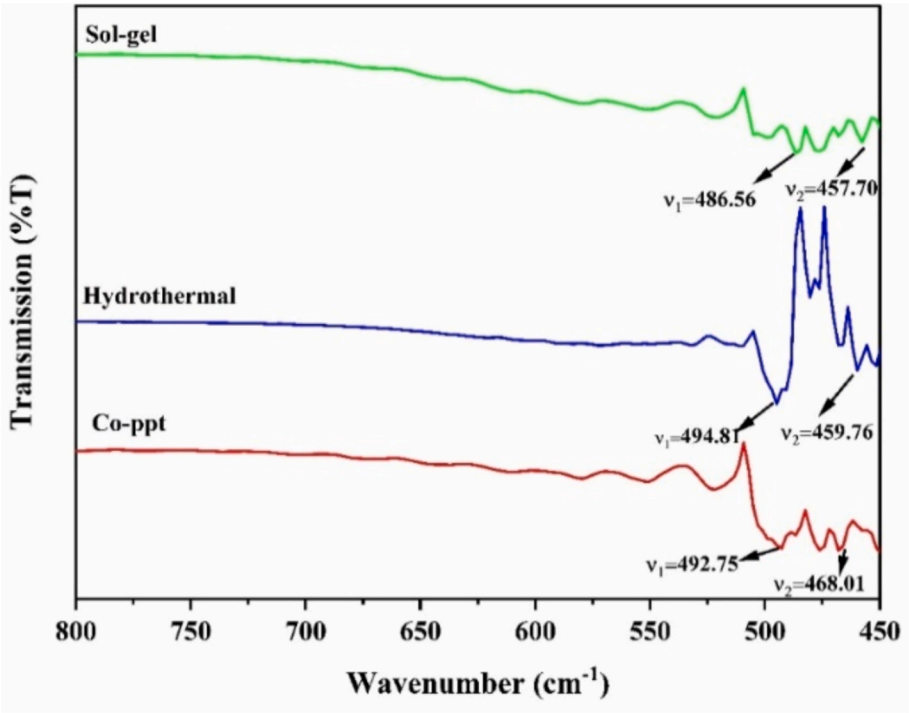

Fig. 2. FTIR spectra of $Mg_{0.2}Ni_{0.6}Zn_{0.2}Fe_2O_4$ SFNPs synthesized with different synthesis approaches.

Table 3
Magnetic parameters retentivity (Mr), saturation magnetization (Ms), coercivity (Hc), squareness ratio, and magnetic moment (η_B) of $Mg_{0.2}Ni_{0.6}Zn_{0.2}Fe_2O_4$ SFNPs synthesized with different synthesis approaches.

Sr. No.	Sample	Mr (emu/g)	Ms (emu/g)	Hc (Oe)	SQR	η_B (μ_B)
1	Sol–gel	1.51	27.48	55.34	0.054	1.126
2	Hydrothermal	3.99	50.64	48.82	0.078	2.075
3	Coprecipitation	1.25	21.23	124.74	0.058	0.87

properties, including coercivity, saturation magnetization, and retentivity. From Fig. 4 It has been observed that hydrothermally synthesized SFNPs shows perfectly smooth S-shaped hysteresis curve with higher value of saturation magnetization and retentivity while the coercivity is smaller compared to others. Research shows that SFNP crystallite size and magnetic properties depend on synthesis method. Sol–gel yields 28.9 nm crystallite size, while hydrothermal yields 20.2 nm. Also, coercivity (Hc) decreases. We observe 55.34 to 48.82 Oe. value of decreasing Hc, which correlates with decreasing crystallite size and supports the Stoner–Wohlfarth theory [13]. Hydrothermal samples have higher M_S, SQR, and Bohr's Magnetron than other samples, which meets the threshold for their future use as biomedical carriers, where saturation magnetization improves Theranostic performance. For coprecipitation, Hc rises for the smallest crystallite size. Because the smaller crystallite has more surface to volume atoms, the surface effect is stronger and structural deformation develops. Super exchange interactions are affected by broken exchange bonds and disordered spins on the exterior surface, causing structural deformation. As the magnetic domain widens, more atomic spins align with the magnetic field, increasing saturation magnetization [18]. Such magnetic parameters are widely applicable for high frequency devices, data storage and

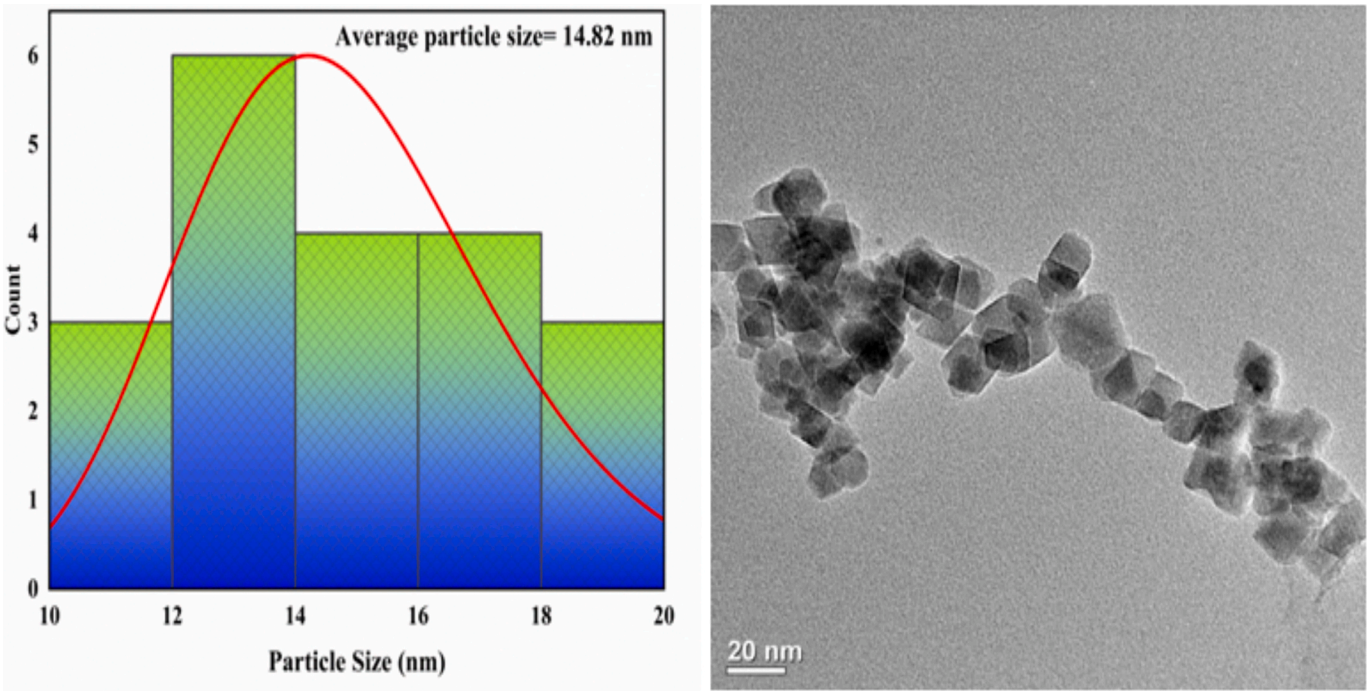

Fig. 3. Lognormal size distribution curve and TEM image of $Mg_{0.2}Ni_{0.6}Zn_{0.2}Fe_2O_4$ SFNPs synthesized with hydrothermal synthesis approach.

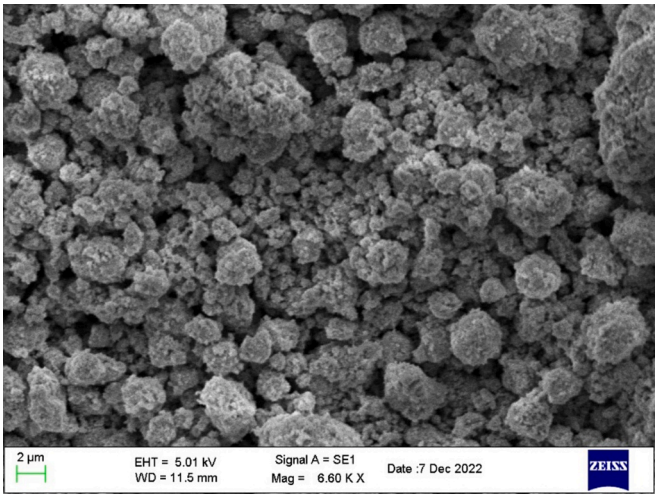

Fig. 4. SEM image of $Mg_{0.2}Ni_{0.6}Zn_{0.2}Fe_2O_4$ SFNPs synthesized with hydrothermal synthesis approach.

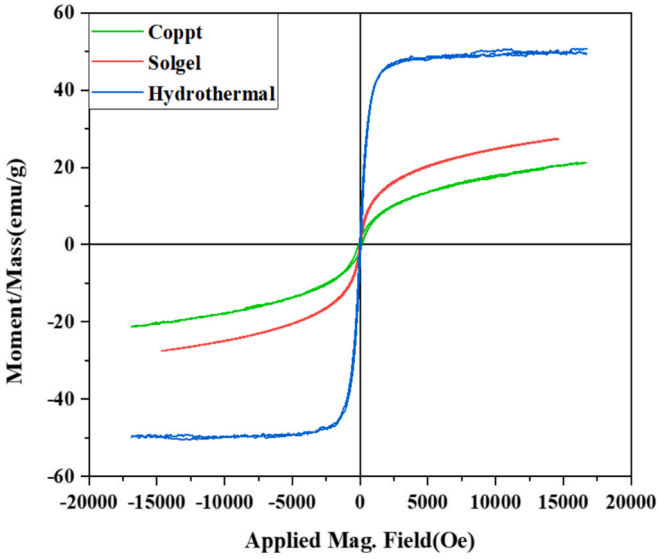

Fig. 5. MH loop of $Mg_{0.2}Ni_{0.6}Zn_{0.2}Fe_2O_4$ SFNPs synthesized with different synthesis approaches.

biomedical applications [30,31]. The magnetic hardness of the prepared SFNPs, was described by squareness ratio (*Mr/Ms*). As previously reported, the Squareness ratio ($0.5 < Mr/Ms < 1$) signifies the more anisotropic, hard, and single-domain nature of nano ferrite. Further, if $0.05 < Mr/Ms < 0.5$ corresponds to the particle interaction by magnetostatic couplings with pseudo-single domain, and $Mr/Ms < 0.05$ signifies the randomly oriented multi-domain nature of the nano ferrite [32]. From Table 3, The obtained squareness ratio (*Mr/Ms*) indicates the pseudo-single domain nature of synthesized SFNPs.

3.4. TEM microstructural analysis

For spinel materials, the morphology is often very predictive of their physical and chemical characteristics [18]. To delve deeper into the surface case's morphology and uniformity, a transmission electron microscope (TEM) is employed. Fig. 3 shows transmission electron micrographs taken of the hydrothermally produced particles, which show that their shape is isotropic. More than 25 distinct particles were measured for the size of spinel ferrite nanoparticles (SFNPs) produced using the hydrothermal technique with the help of Image-j software. Fig. 3 shows the representative TEM pictures with the corresponding size distributions. The consistent cubic structure and a crystal size ranging from 10 nm to 20 nm were further validated by TEM investigation (Fig. 3). A lognormal size distribution was used to fit the histograms, and the average particle size was estimated to be approximately 14.82 nm. The TEM particle sizes corroborate the crystallite sizes determined by the PXRD investigations. Image analysis using transmission electron microscopy reveals a consistent distribution of particle sizes throughout the powder.

3.5. Surface morphology analysis

The Scanning Electron Microscopy (SEM) image of hydrothermally synthesized $Mg_{0.2}Ni_{0.6}Zn_{0.2}Fe_2O_4$ spinel ferrite nanoparticles (SFNPs) illustrates their microstructure and surface appearance, as shown in Fig. 4. The photos display a distinct porous surface and sphero-cubical grains with clearly delineated grain borders and sharp edges. The grains were predominantly uniformly distributed, while some agglomerated patches were seen in certain areas. This aggregation may be attributed to the interaction of magnetic nanoparticles [18].

4. Conclusion

Sol–gel auto-combustion, hydrothermal, and coprecipitation methods were used to prepare polycrystalline multi-metal $Mg_{0.2}Ni_{0.6}Zn_{0.2}Fe_2O_4$ spinel ferrite nanoparticles. Crystallinity, structural, optical, and magnetic properties of prepared SFNPs varied. XRD pattern matches cubic spinel structure (MFe_2O_4) with space group fd-3 m. Sol–gel auto-combustion, hydrothermal, and coprecipitation techniques yielded 28.9, 20.2, and 7.5 nm crystallite size. FTIR spectra show two absorption bands at 500 cm^{-1} and 450 cm^{-1}, confirming metal–oxygen bonding in spinel ferrite. However, the synthesis method shifts the tetrahedral and octahedral bands. Surface morphology of hydrothermally produced SFNPs was investigated using SEM and TEM, confirming their homogeneous cubic structure and 14.82 nm mean particle size. Sample VSM data showed that coprecipitation method has highest coercivity and hydrothermal method has lowest, with maximal saturation magnetization and smooth S-shaped hysteresis curve. Thus, the hydrothermal method is better for synthesizing spinel ferrite nanoparticles with controlled crystallite size and superparamagnetic performance for hyperthermia, high-frequency devices, high-density recording, ferrofluids, and magnetic refrigerators.

CRediT authorship contribution statement

Sarang R. Daf: Writing – original draft, Methodology, Investigation, Formal analysis, Conceptualization. **Dilip S. Badwaik:** Writing – review & editing, Supervision, Project administration, Investigation, Formal analysis, Data curation. **Shrikant M. Suryawanshi:** Writing – review & editing, Validation, Software, Resources, Formal analysis. **Bhupendra T. Kumbhare:** Methodology, Investigation, Formal analysis, Data curation. **Bhaurao R. Balbudhe:** Visualization, Validation, Software. **Rupesh S. Wandhare:** Writing – review & editing, Writing – original draft, Software, Investigation.

Declaration of competing interest

The authors declare that they have no known competing financial interests or personal relationships that could have appeared to influence the work reported in this paper.

Acknowledgment

The authors gratefully acknowledge CIC, Shri Shivaji Science College, Amravati for the XRD and SIL, Department of Physics, Shri Shivaji Science College, Nagpur for FTIR facilities, NEHU Shillong for TEM and IIT Guwahati for VSM.

Data availability

Data will be made available on request.

References

[1] N. Adarshgowda, et al., Green synthesized manganese-doped cobalt ferrite photocatalysts for light driven degradation of dye and optoelectronic studies, *Ceram. Int.* 50 (12) (2024) 22060–22076, https://doi.org/10.1016/j.ceramint.2024.03.320.
[2] Wu, Xuehang, et al., Structure and magnetic properties evolution of nickel–zinc ferrite with lanthanum substitution, *J. Magn. Magn. Mater.* 379 (2015) 232–238, https://doi.org/10.1016/j.jmmm.2014.12.057.
[3] G. Vinod, K. Rajashekhar, J. Laxman Naik, Dysprosium doped Cu0. 8Cd0. 2DyxFe2-xO4 nano ferrites: A combined impact of Dy3+ on enhanced physical, optical, magnetic, and DC-electrical properties, *Ceram. Int.* 49 (2) (2023) 2829–2851.
[4] Hcini, Fakher, et al., Thermal, microstructural, optical, magnetic and magnetocaloric studies for Ni0. 5Mn0. 5Cr2O4 chromite spinel prepared using sol–gel method, *J. Mol. Struct.* 1243 (2021) 130769.
[5] M.K. Raju, et al., Physical characterization, magnetic interactions and DC electrical resistivity properties of La3+ substituted NiZnCd nano ferrites, *Inorg. Chem. Commun.* 163 (2024) 112274, https://doi.org/10.1016/j.inoche.2024.112274.
[6] Ikram, Salma, et al., Influence of Ce3+ substitution on the structural, electrical and magnetic properties of Zn0. 5Mn0. 43Cd0. 07Fe2O4 spinel ferrites, *Physica B Condens. Matter.* 580 (2020) 411764, https://doi.org/10.1016/j.physb:2019.411764.
[7] D. Parajuli, et al., Study of structural, electromagnetic and dielectric properties of cadmium substituted Ni–Zn nanosized ferrites, *J. Indian Chem. Soc.* 99 (3) (2022) 100380.
[8] Hossen, M. Moazzam, M. Belal Hossen, Structural, electrical and magnetic properties of Ni0. 5Cu0. 2Cd0. 3LaxFe2-xO4 nano-ferrites due to lanthanum doping in the place of trivalent iron, *Physica B Condens. Matter.* 585 (2020) 412116.
[9] Reyes-Rodríguez, Pamela Yajaira, et al., Structural and magnetic properties of Mg-Zn ferrites (Mg1−xZnxFe2O4) prepared by sol–gel method, *J. Magn. Magn. Mater.* 427 (2017) 268–271, https://doi.org/10.1016/j.jmmm.2016.10.078.
[10] Tatarchuk, Tetiana, et al., Synthesis, morphology, crystallite size and adsorption properties of nanostructured Mg–Zn ferrites with enhanced porous structure, *J. Alloys Compd.* 819 (2020) 152945, https://doi.org/10.1016/j.jallcom.2019.152945.
[11] B. Rabi, et al., Structural, optical and dielectric properties of nickel zinc spinel ferrites synthesized by co-precipitation method, *Journal of Materials Science: Materials Electronics* 32 (2021) 932–943.
[12] Jasrotia, Rohit, et al., Magnetic and electrical traits of sol–gel synthesized Ni-Cu-Zn nanosized spinel ferrites for multi-layer chip inductors application, *J. Solid State Chem.* 289 (2020) 121462.
[13] Daf, R. Sarang, et al., Effect of hydrothermal processing duration on physical and antimicrobial properties of Mg0.2Zn0.5Mn0.3Fe2O4 ferrite nanoparticles, *Mater. Sci. Eng. B* 298 (2023) 116879, https://doi.org/10.1016/j.mseb.2023.116879.
[14] P.S. Hedaoo, et al., Structural and magnetic studies of Zn doped nickel nanoferrites synthesized by sol–gel auto-combustion method, *Mater. Today Proc.* 15 (2019) 416–423, https://doi.org/10.1016/j.matpr.2019.04.102.
[15] Majid, Farzana, et al., Synthesis and characterization of $NiFe_2O_4$ ferrite: sol–gel and hydrothermal synthesis routes effect on magnetic, structural and dielectric characteristics, *Mater. Chem. Phys.* 258 (2021) 123888, https://doi.org/10.1016/j.matchemphys.2020.123888.
[16] Balbudhe, Bhaurao R., et al. "Structural and magnetic investigation on Cr3+ substituted Mn0. 25Cu0. 25Zn0. 5Fe2O4 nano ferrites by co-precipitation route."*IOP Conference Series: Earth and Environmental Science*. Vol. 1281. No. 1. IOP Publishing, 2023.
[17] Comparative Studies of Spinel MnFe2O4 Nanostructures: Structural, Morphological, Optical, Magnetic and Catalytic Properties, A. Mary Jacintha1, A. Manikandan2, K. Chinnaraj1, S. Arul Antony2, and P. Neeraja3_*.
[18] Daf, R. Sarang, et al., Physical, spectroscopic and antibacterial investigation of Mg0. 3Zn0. 5Mn0. 2Fe2O4 via temperature dependent hydrothermal approach, *J. Magn. Magn. Mater.* 567 (2023) 170346, https://doi.org/10.1016/j.jmmm.2022.170346.
[19] P. Tiwari, et al., Effect of Zn addition on structural, magnetic properties and anti-structural modeling of magnesium-nickel nano ferrites, *Mater. Chem. Phys.* 229 (2019) 78–86.
[20] S.G. Bachhav, et al., Microstructure and magnetic studies of Mg–Ni–Zn–Cu ferrites, *Mater. Chem. Phys.* 129 (3) (2011) 1104–1109.
[21] N. Fortas, et al., Effect of Ni substitution on the structural, magnetic and magnetocaloric properties of Zn0. 5-xNixMg0. 5Fe2O4 (x= 0, 0.125 and 0.250) ferrites, *Solid State Sci.* 101 (2020) 106137, https://doi.org/10.1016/j.solidstatesciences.2020.106137.
[22] P.M. Sontakke, et al., Structural and Magnetic investigation of Cu2+ substituted Mn-Zn spinel ferrite synthesized using hydrothermal route, *International Journal of Architecture, Engineering and Construction* 11 (2) (2022) 61–73.
[23] P.S. Hedaoo, D.S. Badwaik, K.G. Rewatkar, Morphological study and optoelectrical properties of Zn2+ substituted nickel ferrite nanoparticles, *Mater. Today Proc.* 29 (2020) 1033–1038.
[24] Suryawanshi, M. Shrikant, et al., Structural, surface, magnetic, and dielectric properties of Ni0. 3Cu0. 3Zn0. 4Fe1. 4Cr0. 6O4 spinel ferrite nanocrystals prepared by sol–gel auto combustion route, *Inorg. Chem. Commun.* 156 (2023) 111204, https://doi.org/10.1016/j.inoche.2023.111204.
[25] Balbudhe, R. Bhaurao, et al., Structural and magnetic behaviour of temperature influenced Mn0. 5Zn0. 25Cu0. 25Fe2O4 spinel nanoparticles by co-precipitation route, *J. Mater. Sci. Mater. Electron.* 35 (12) (2024) 818, https://doi.org/10.1007/s10854-024-12484-w.
[26] Yadav, Raghvendra Singh, Ivo Kuřitka, Jarmila Vilcakova, Jaromir Havlica, Jiri Masilko, Lukas Kalina, Jakub Tkacz, Vojtěch Enev, Miroslava Hajdúchová, Structural, magnetic, dielectric, and electrical properties of NiFe2O4 spinel ferrite nanoparticles prepared by honey-mediated sol–gel combustion, *J. Phys. Chem. Solids.* 107 (2017) 150–161.

[27] D.H. Bobade, S.M. Rathod, M.L. Mane, Sol–gel auto-combustion synthesis, structural and enhanced magnetic properties of Ni2+ substituted nanocrystalline Mg–Zn spinel ferrite, *Phys. B Condens. Matter* 407 (18) (2012) 3700–3704.
[28] N. Shamgani, A. Gholizadeh, Structural, magnetic and elastic properties of Mn0. 3− xMgxCu0. 2Zn0. 5Fe3O4 nanoparticles, *Ceram. Int.* 45 (1) (2019) 239–246.
[29] P. Tiwari, et al., Effect of Zn addition on structural, magnetic properties and anti-structural modeling of magnesium-nickel nano ferrites, *Mater. Chem. Phys.* 229 (2019) 78–86.
[30] Nandanwar, D. V., et al. "A review on highly versatile electromagnetic material: Mg spinel ferrites." *AIP Conference Proceedings*. Vol. 2974. No. 1. AIP Publishing, 2024.
[31] S.M. Suryawanshi, D.S. Badwaik, B.S. Shinde, K.D. Gaikwad, M. Shkir, K. V. Chandekar, S. Gundale, A comprehensive study on structural, magnetic and dielectric properties of Ni0. 3Cu0. 3Zn0. 4Fe1. 8Cr0. 2O4 nanoparticles synthesized by sol–gel auto combustion route, *J. Mol. Struct.* 1272 (2023) 134173, https://doi.org/10.1016/j.molstruc.2022.134173.
[32] V.V. Warhate, D.S. Badwaik, Structural, magnetic and thermo-magnetic properties of NiMn Y-Type strontium nano-hexaferrites, *J. Alloys Compd.* 818 (2020) 152830.

Further reading

[33] A.V. Gongal, et al., Study on multifunctional magnesium copper zinc spinel ferrite nanoparticles prepared by hydrothermal route; Physical, electrical, and anti-microbial investigation, *Nano-Struct. Nano-Objects* 39 (2024) 101248.